Population Kinetics of a Repetitively-Pulsed Nanosecond Discharge

by

Benjamin T. Yee

A dissertation submitted in partial fulfillment
of the requirements for the degree of
Doctor of Philosophy
(Nuclear Engineering & Radiological Sciences)
in the University of Michigan
2013

Doctoral Committee:

Associate Professor John E. Foster, Chair
Doctor Edward V. Barnat, Sandia National Laboratories
Doctor Isaiah M. Blankson, National Aeronautics and Space Administration
Professor Augustus Evrard
Professor Mark J. Kushner

2013

I would like to dedicate this dissertation to someone else.

A C K N O W L E D G M E N T S

Who is this?

Preface

This is a dissertation about something; I really hope it's good.

TABLE OF CONTENTS

LIST OF FIGURES

LIST OF TABLES

LIST OF APPENDICES

LIST OF ABBREVIATIONS

RPND repetitively-pulsed nanosecond discharge

APP atmospheric-pressure plasma

EEDF electron energy distribution function

FIW fast ionization wave

LAS laser-absorption spectroscopy

LCIF laser collision-induced fluorescence

MHD magnetohydrodynamic

FWHM full-width half maximum

FID fast ionization dynistor

MIPT Moscow Institute of Physics and Technology

CCD charge-coupled device

CHAPTER 1

Introduction

1.1 Overview

1.1.1 Motivation

Plasmas, commonly called the fourth state of matter, are a gas where a significant fraction of the neutral atoms or molecules have been split into pairs of electrons and positive ions. Initially, a curiosity of the laboratory, they have become a critical part of every day life. The electrically charged nature of plasmas makes them a practical means by which to convert electrical energy into light, chemical reactions, kinetic energy, or even nuclear reactions. From an applications perspective, they are indisposable in lighting, semiconductor manufacturing, plastic processing, and space propulsion. On a more broad scale, virtually all observable light in the universe is the result of a plasma in some form or another.

Some exceptions aside, only three things are required to create a plasma: a gas, an energy source, and a means of transferring the energy to the gas. In man-made applications, the energy source is typically electricity, and the simplest transfer mechanism are two electrodes placed on either side of the gas. This results in an electric field in the gap between the electrodes, as seen in figure 1.1. The field accelerates a single seed electron in the gas (often created by background cosmic radiation) until it collides with a neutral particle. The electron, having acquired a fair amount of energy, knocks a second electron loose from the particle, leaving behind a relatively heavy and immobile ion. Subsequently, both the first

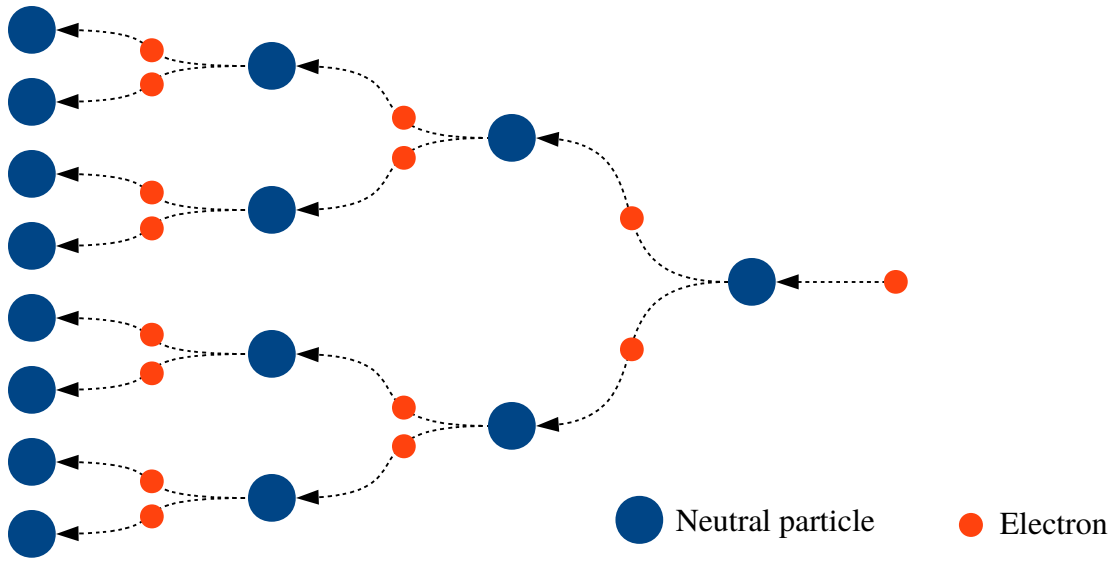

Figure 1.1: A simplified depiction of the avalanche breakdown process in a gas.

and second electron are now accelerated by the electric field. Again, they collide with two more neutral atoms, creating two new electrons. As long as the electric field persists, the number of electron and ion pairs increases exponentially. This process is generally referred to as an avalanche.

Despite this relatively simple recipe, the physical characteristics can vary greatly depending on what gas is used, what pressure it is at, what voltage is used, whether the electricity is applied constantly or varied over time, what kind of electrodes are used, etc. As a result, man-made plasmas are generally produced under very specific conditions. For example, a plasma etcher used in semiconductor manufacturing may need to operate operate at pressures that are one-thousandth of atmospheric pressure with ultra-pure (99.9999%) gases.

Plasmas like those which occur in plasma etchers, feature ions and neutral gas particles with temperatures that are below 1,000 K, or roughly 1,340° F. Though this temperature is relatively high compared to room temperature, it is well below the temperature of the electrons which may be in excess of 20,000 K. Plasmas which exhibit this disparity in temperatures are often called nonequilibrium or “low-temperature” plasmas.

Conversely, there exists another class of plasmas where the electrons, ions, and neutral particles are all at the same temperature. These are called thermal plasmas. Generally speaking, the closer the gas pressure is to atmosphere, the more thermal a plasma is. Additionally, the temperatures in a thermal plasma can be quite high and, in many cases, can easily melt most metals. For example, the arc of an arc welder is a thermal plasma. Similar high temperature plasmas, have a number of other applications which include a variety of high-intensity lamps, metal cutting, and surface coating.

There are, however, a number of applications which would benefit from operation at higher pressures, but with low-temperature ions and neutrals so as to avoid heat damage. This has spurred a substantial amount of research on nonequilibrium atmospheric-pressure plasmas (APPS) in recent years. Ideally, such a plasma could be generated at or near atmospheric pressure with hot electrons, but minimal heating of surrounding gas. Though this field of research is still relatively young, it has produced a variety of new plasmas and capabilities. One of the more ubiquitous examples is use of plasmas to process the surface of plastics so that ink can adhere. Separately, nonequilibrium APPS are the technology which drives plasma televisions.

As mentioned, these applications promise to be the first of many for such plasmas. More recently, there have been innovative proposals to use these plasmas in water purification, wound sterilization, improved combustion engines, nanoparticle production, and more. However, each situation has its own challenges when it comes to the design and development of a plasma source, particularly at these elevated pressures. Particularly problematic is the tendency of APPS to develop instabilities which can cause them to rapidly transition to thermal plasmas in a matter of nanoseconds.

There exist a few ways of getting around these instabilities. One example is the dielectric-barrier discharge which passively regulates the amount of power which can be deposited into the plasma. Another example includes split-ring resonators which use natural feedback mechanisms to damp out potential instabilities. The technique considered here, referred to

as the repetitively-pulsed nanosecond discharge, or RPND, uses high voltage pulses which are so short that the instability does not have time to develop. The RPND is a nonequilibrium plasma which can operate at pressures ranging from approximately 10^{-3}–10 atmospheres. At atmospheric pressure the RPND can produce a uniform plasma in volumes on the order of 10 mL. As the pressure is reduced, the plasma volume can reach the order of liters.

The importance of large-area, uniform, high-pressure plasmas such as the RPND was highlighted in the National Academies' most recent decadal survey of plasma science [3]. However, there is still much that is not know about such plasmas. From the same survey, it is said that "the full promise of APPS will be known only if they can be understood and managed based on fundamental scientific principles at two extremes–the nanoscopic kinetic level, where selective chemistry occurs, and the global stability level." It is this challenge, specifically the investigation of the nanoscopic kinetic level, which drives the research presented here.

1.1.2 History

Historically, the study of low-temperature APPS has been almost indistinguishable from the study of plasmas as a whole. However, this was not necessarily a matter of reasoned choice. Plasma generation at atmospheric-pressure obviates the need for an effective vacuum pump. Additionally, prior to the creation of large battery banks, early sources of electrical energy had relatively small capacities. This precluded the generation of thermal atmospheric plasmas which required large amounts of energy.

Indeed, the requirements for a low-temperature APP are sufficiently rudimentary that the first man-made one (and likely the first man-made plasma), was probably a spark generated by rubbing fur against amber. This is commonly attributed to Thales of Milêtus from around 600 B.C. Following Thales, electrical sparks came to intrigue many scientists including Gottfried Liebniz, Benjamin Franklin, and Charles Wheatstone. By the mid-1800s, Plücker, Geißler, and Hittorf began some of the first work on low-pressure plasmas though it was

Crookes who would later identify plasma as a separate state of matter. Later, J.J. Thomson's discovery of the electron and discretized charge in 1897 marked the beginning of modern plasma research.

By this time, the necessary tools and techniques existed to create steady plasmas in pure, rarified gases. The behaviors of which were dominated by the motion and interaction of the charged electrons and ions. Critically, the effects of the neutral particles were negligible, thus isolating the electrical properties of the plasma. These carefully controlled systems were ideal for basic studies of plasma behavior and were used to great effect by individuals such as Irving Langmuir and Lewi Tonks. In fact, many modern concepts in plasma physics can be traced back to their work.

In contrast, the pulsed APPs, characteristic of the earliest man-made plasmas, were easy to create, but notoriously difficult to work with. It could take them only a few nanoseconds to form, and less than a millisecond to decay away. For many years, there were simply no instruments capable of taking measurements this quickly. Furthermore, the neutral particles which were of no consequence in the low-pressure plasmas, could not be ignored. The neutral particles were present in such quantities that they could confound or obscure otherwise simple measurements.

As a consequence, there is still a great deal that is not known about about pulsed APPs, particularly lightning, streamers, and a type of plasma which Thomson referred to as a "luminous front." By the 1970s, this latter plasma had come to be called the fast ionization wave, or FIW. It was generated by a single voltage pulse lasting around 100 nanoseconds and peaking at 10s or 100s of kilovolts. For the right pressure and gas, the FIW could fill volumes of nearly 40 L with a relatively uniform plasma, but with little heating of the gas.

These properties were attractive for a number of uses, but the FIW faced a number of implementation-related challenges. The switches used to trigger the FIW could only operate up to 100 times each second. Unfortunately, the lifetime of a plasma at elevated pressures is relatively short, and the plasma generated by the FIW would decay away quickly after

each pulse. This meant that the FIW-generated plasma had a relatively low duty cycle; the ratio of the time the plasma spends on to the time it spends off. This was disadvantageous for plasma-processing applications where low duty cycles are equivalent to long processing times. The low duty cycle also necessitated so-called preionization of the gas with UV lamps or a secondary plasma generator, adding to the cost and complexity of the system. Finally, the pulse generators used for FIWS were not considered reliable enough for long operational lifetimes.

Recent advances in solid-state switching technology has largely solved these issues. At present, switches exist which can reliably operate 100,00 times a second; sufficiently fast that the plasma duty cycle approaches 100%. This has the additional benefit of obviating the need for a preionization stage, as a sufficient number of electrons persist between pulses. The discharge produced by the use of these new switches is what we refer to as the RPND.

1.1.3 Questions

The large pedigree of pulsed plasma research belies the fact that they are still not well-understood. This remains especially true for RPNDS which present significant experimental challenges. A major component of this has to do with the time scales associated with the RPND. The formation of a RPND often requires no more than 10-20 nanoseconds. Very sensitive equipment is required in order to measure changes which occur during this period. Unfortunately, such equipment is particularly susceptible to the broadband electronic noise generated by the fast pulses. There is a plethora of other problems that can be traced back to topic of timing. For example, things like the length and insulators of detector cables can introduce substantial delays, and must be considered in order to synchronize different measurements.

Consequently, the majority of RPND studies focus on measurements after the discharge has occurred, when changes happen at a much slower rate. A great deal of information is available for this period of time, including chemical compositions, atomic densities, electron

densities, gas temperatures, and more. While undoubtedly important, these measurements provide limited insight on what is happening *while* the plasma is forming. It is natural, then, to ask, what are the RPND plasma properties during formation?

Additionally, most studies have used a limited range of gases: oxygen, nitrogen, air, hydrogen, or some mixture thereof. The choice of these gases is deliberate and reflects specific applications in combustion and aerospace. However, the use of rare gases (such as helium) and rare gas mixtures has become popular because they provide for a wider range of stable operating conditions. Notably, it has been found that unique internal structures of rare gases can produce very different discharges. Given this, there is the question of how rare gas RPNDs compare to more conventional ones.

Finally, the persistence of the plasma between pulses makes the development of a RPND very different from a FIW. One reason for this is the large number of electrons that remain between pulses in the RPND. While these seed electrons are necessary for the discharge to develop, in too large a number they can shield out the applied pulse. This can have the detrimental effect of reducing the final plasma density. These competing effects have to be balanced in order to obtain an optimal result, and what is considered optimal can vary depending on the application. Therefore, one must ask how the properties of a RPND compare to a similar FIW and how they vary depending on the operating conditions.

1.1.4 Approach

The dissertation presented here represents my efforts to either answer or provide a foundation to answer these questions. In order to develop the appropriate context for this work, the next section will be a comprehensive review of the RPND literature. It begins with the first reported pulsed APPS and concludes with contemporary studies.

The following two chapters set the basis for the experimental and numerical studies. Chapter 2 presents the theory necessary to understand RPNDs including streamer discharges, atomic spectroscopy, and collision processes. Subsequently, chapter 3 describes the design

of the helium RPND discharge apparatus used for the experimental studies and as the basis for the simulations. Also included in this chapter are several measurements of the basic discharge properties.

Chapters 4 through 6 provide more detailed measurements and analysis of the RPND dynamics. In chapter 4, the measurements of the helium metastables in a RPND are presented and analyzed as a function of pressure an axial location in the discharge apparatus. Chapter 5 presents and analyzes similar measurements of the spontaneous plasma emissions. Finally, chapter 6 discusses the development of a global model for a helium plasma and its use with the experimental data to infer the plasma properties of the RPND. The dissertation concludes with a summary of the results and suggestions for further avenues of research.

1.2 Literature Review

RPNDS are only a recent invention which resulted from advances in fast-switching semiconductors. However, the physics of their formation is related to a much more broad category of plasmas which includes lightning, streamers, and even some transient phenomena in DC glows [4]. These plasmas are unique in that their spatial structure develops at speeds much faster than can be accounted for by the conventional Townsend mechanism. Loeb refers to this phenomena as "ionizing waves of potential gradient." [1].

1.2.1 Early History of Pulsed Discharges

In 1835 (as reported by Thomson [5]), Charles Wheatstone attempted to measure what he thought to be the speed of electricity between two electrodes, connected by a vacuum tube, six feet in length [6]. It is now known that he was actually measuring the speed with which a plasma formed between the two electrodes. He accomplished this by the use of a rotating

[1] It should be noted that the phrase wave does not indicate any kind of periodic motion or spatial arrangement. Simply put, it describes a boundary which separates ionized and unionized gas which travels from one electrode to another.

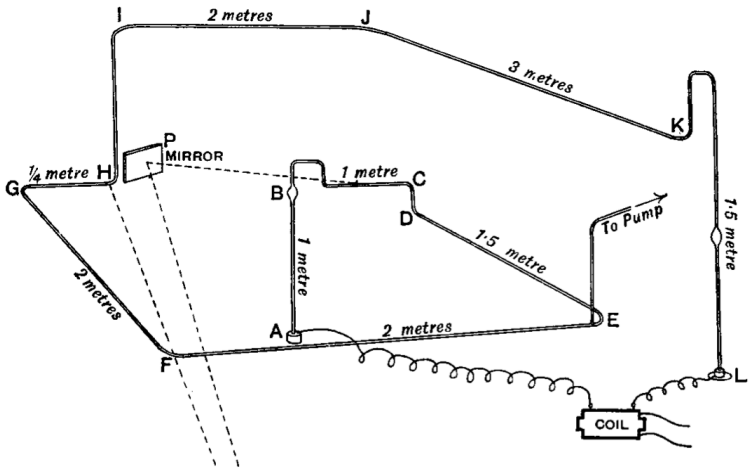

Figure 1.2: A sketch of J.J. Thomson's early experiments on pulsed plasmas in long vacuum tubes.

mirror which allowed him to see images of two sections of the tube, slightly displaced. The displacement between the images was proportional to the speed with which the plasma traveled between them. Wheatsone estimated this speed to be at least 8×10^7 cm/s.

Interestingly, von Zahn later noted that this was *not* the speed of the emitting particles [7]. That is, even though the visible light crossed the electrode gap at a high speed, the particles did not.

Later, Thomson revisited this work with an improved apparatus [5]. This included a tube that was now 15 m in length and five mm in diameter, as seen in figure 1.2. Also using the rotating mirror apparatus, Thomson was able to greatly improve on the estimates of Wheatstone. He estimated that the so-called "luminous front" had a speed that was more than 1.5×10^{10} cm/s, or in excess of half of the speed of light. Furthermore, Thomson determined that the luminous front always appeared to travel from the positively pulsed electrode (anode) to the ground electrode (cathode).

The study of these luminous fronts was revisited by several researchers in the wake of Thomson [8–10], but their attempts to duplicate the measured speeds were met with varied success. In 1930, Beams confirmed definitively confirmed those of Thomson. He also discovered that the front always traveled from the electrode with the highest absolute

potential, to the lowest one. In other words, it could be anode *or* cathode directed, depending on the magnitude of their potentials relative to ground. Beams hypothesized that the rapid motion of the front was a result of a self-propagating region of high space charge, quote:

> In the neighborhood of the electrode . . . the field is very high and intense ionization should take place. This ionization due to the large difference in mobilities of positive ions, negative ions and electrons respectively should result in the establishment of a space charge. This space charge, once formed near the high potential electrode . . . must move down the tube regardless of the polarity of the applied potential because of the changes it produces in the field near its edges.

At about the same time, Schonland and Collens reported on their observations of lightning [11]. Though the general structure and length scale of lightning is substantially different from the luminous fronts observed by Beams and Thomson, the two phenomena would later prove to be very similar. In their work Schonland and Collens noted that lightning would usually occur in a two-step process. Based on the images they obtained, they suggested that the leader was generated by a relatively small "dart" with a mean vertical velocity of 7.2×10^8 cm/s. The dart moved in a random manner, changing directions at random intervals, but always moving toward the ground.

The second step began when this dart reached the ground. Once there, a bright return stroke would occur along the same path that the leader had traced out. In contrast to the leader stroke, the return stroke had a velocity of 5×10^9 cm/s. Schonland and Collens hesitantly attributed the leader stroke to an extended electron avalanche, and the return stroke to thermal ionization along the conductive path generated by the dart. However, calculations by Cravath and Loeb showed that the speeds of the proposed avalanche was inconsistent with the fields at the head of a lightning stroke [12]. Instead, they suggested that the dart was actually a moving region of space charge which locally accelerated electrons to ionizing energies. This was similar to the mechanism earlier proposed by Beams.

1.2.2 The Streamer Model

It was long known that sparks in air were similar to lightning. Advances in technology during the 1930's led to experiments which reinforced this similarity. In response to the measurements of Schonland and Collens; Snoddy, Beams, and Dietrich studied the breakdown of gas in a long tube with both positive and negative applied potentials [13]. Using an oscillograph, they observed both the leader and a return stroke in both cases. However, the propagation of the plasma wave toward the cathode required a source electrons ahead of the wave. The authors proposed that photoionization might provide these necessary electrons.

Around the same time, Flegler and Raether had come to a similar conclusion regarding the importance of photoionization. This led them to develop a more thorough theoretical model for these waves [14] which came to be known as the streamer theory. This was followed by a similar treatment by Loeb and Meek [15–17]. The streamer theory divided the initial plasma formation into two steps. In the first step, an electron avalanche is initiated between two electrodes. The avalanche travels toward the anode and leaves behind a region of positive space charge. In the second step, the return stroke begins at the anode and travels along the conductive path generated by the initial avalanche toward the cathode.

The streamer model proved relatively successful in describing the development of sparks and lightning. Theoretical estimates of the speed matched the velocity measurements that were acquired with photographs and oscillographs. Additionally, the theory was able to account for the halting manner in which lightning was formed as well as the constriction in space.

Following the initial work of Flegler, Raether, Loeb, and Meek, a number of researchers began to explore the boundary between the Townsend mechanism and the streamer mechanism. Most notable was Fisher and Bederson's work in 1951 [18], which was later extended to nitrogen [19] and argon [20]. These studies suggested that the streamer theory was incomplete. Furthermore, the reliance of the streamer theory on photoionization would later prove very contentious [21]. Finally, there was a whole class of discharges that it did not

readily explain.

1.2.3 Diffuse Streamers

Per Chalmers [22], Rogowski and Buss [23, 24] observed a fast, diffuse, glow discharge immediately prior to the filaments of a streamer discharge. Allibone and Meek, noted similar diffuse discharges in air based on oscillographs and photographs [25–27]. However, the Boys apparatus which was employed in these studies (an ancestor to the modern streak camera) was unable to capture the evolution of the diffuse glow, given its large spatial extent.

This was first noted by Allibone who attempted to use Lichtenberg figures[2] to definitively capture this diffuse glow [28]. Later, Saxe and Meek used the recently invented photomultiplier tube to record the evolution of the light emissions in the brief, diffuse glow [29] as a function of space. Both studies agreed in the existence of the diffuse glow, despite some disagreement on the nature of its geometry and propagation.

By 1968 (according to Kunhardt and Byszewski [30]), Stankevich and Kalinin had provided the most firm evidence yet of a diffuse discharge in a dense gas [31]. This was later confirmed by experiments with a pulsed nanosecond discharge by Mesyats, Bychkov, and Kremnev [32]. In their analysis, they noted that photoionization could not play a role in such short-lived discharges and thus there was a need for extensions to the streamer model.

In addition to the diffuse discharge, Stankevich and Kalinin also noted the detection of x-rays with each pulse. This suggested the presence of high-energy electrons impinging on the surface of the electrodes, despite the high collisionality of the dense gas. Not only that, but the electron energies could even exceed what would be expected from the vacuum electric fields [33]. The eventual conclusion was that the electric field associated with the space charge at the head of the streamer produced very energetic electrons which deposited their energy far from the streamer tip [30, 34], allowing the streamer to spread out beyond

[2]Such figures directly exposed photographic emulsions to the electrical discharge. The developed image was a time-integrated representation of the discharge.

the diffusive region of the electrons.

It was based on the studies of the fast electrons in these discharges that Mesyats, Bychov, and Kremnev proposed the use of a fast electron beam for pumping high-pressure gas lasers. Similar work was conducted simultaneously by «««< HEAD Fenstermacher et al. [35]. Palmer [36], and Levatter and Lin [37] determined that there was a threshold amount of preionization required to ensure homogeneity of the discharge. Hunter [38], and Koval'chuk and Mesyats [39] later proposed that such discharges be used for fast-closing switches. Gas lasers and fast switches would drive much of the later research on fast, pulsed discharges.

Eventually these discharges came to be referred to as fast ionization waves (FIWS). A large body of Russian literature developed around their study, though much of it has remained untranslated. In 1994, Vasilyak produced an extensive review of these studies [40]. The data include wave velocities for a variety of gases and pressures. Other parameters such as attenuation coefficients for the waves, high energy electron currents, electric field measurements, and a circuit model of the FIW are also included.

1.2.4 RPNDS

Beginning in 1998, the Moscow Institute of Physics and Technology (MIPT) produced a flurry of studies on the FIW [41–43]. They employed several different diagnostic techniques (photomultiplier tubes and capacitive probes) in an exceptionally detailed study in both air and nitrogen, using a shock tube and a bell jar. A summary of these investigations can be found in [44]. The work showed exceptionally reproducibility of the discharge parameters at relatively low repetition rates, on the order of tens of Hz, and evidence of runaway electrons. This work also included some of the first approximations of the electron energy distribution function (EEDF).

Interestingly, later analysis of a anode-directed FIW in nitrogen by the group at MIPT [45] concluded that the, the vast majority of the electrons were generated *after* the wave. This

suggests that the ionization in an FIW does not strictly track the luminous front of the wave. Additionally, measurements of the conductivity suggested that the local approximation becomes invalid in the wave front and the electron energy distribution function resembles a beam.

In 1997 the invention of the fast ionization dynistor (FID) was revealed [46]. These new devices enabled sub-nanosecond switching of 10's of kilovolts, with repetition rates approaching 100 kilohertz. This was a leap forward over previous technologies which generally used thyristors or spark gaps for switching. Particularly appealing was the high repetition rate of the FID.

Recall that the volume-filling FIW required a significant amount of preionization. This was often accomplished an ionization source in addition to the high voltage pulse (in the form of UV radiation, or electron beams). However, the repetition rates of FIDs were high enough such that a substantial number of electrons would carry over between pulses. These seed electrons obviated the need for a preionization. In addition, the time-averaged densities of excited states could maintained at much higher values. This had particular promise for processing applications.

In the eventual commercialization of the FID made economically feasible to create fast, repeatable fast ionization waves. It is this class of discharges which are now referred to as repetitively-pulsed nanosecond discharges, or RPNDS. Their uniformity, low gas heating, high-pressure operation, and efficient ionization made them attractive or a number of applications:

- plasma-assisted combustion [47],
- magneto-hydrodynamic energy bypass [48],
- plasma actuators [49],
- and high-pressure xenon lamps [50, 51].

As with the FIWs, the primary diagnostics were current and voltage characteristics, electric field measurements with capacitive probes, and emission measurements with photomultiplier tubes. Later, intensified CCDs were used to record the emissions of specific transitions as well as broadband light. This approach has been used to more clearly illustrate the uniformity and reproducibility of the discharge [49]. Other researchers have turned to laser-based diagnostics, such as coherent anti-Stokes Raman scattering, to measure gas heating [52] and the electric field in molecular systems [53, 54]. Likewise, laser collision-induced fluorescence (LCIF) has been used to obtain axial profiles of excited state and electron densities in helium RPNDs [55].

Concurrent with these improvements in experimental techniques has been similar progress in the simulation of RPNDs. The one-dimensional models

======= Fenstermacher et al. [35]. Later, Hunter [38], and Koval'chuk and Mesyats [39] proposed that such discharges be used for fast-closing switches. The need for a homogeneous plasmas in these applications prompted Palmer [36], and Levatter and Lin [37] to investigate the necessary conditions for uniformity. They concluded that the primary requirement for uniformity was a threshold value of fractional ionization.

1.2.5 Repetitively-Pulsed Nanosecond Discharges

The type of discharge originally studied by Babich, Loika, and Tarasova came to be known as the fast ionization wave (FIW). In the years following its discovery, a substantial effort was made to document the properties of the FIW over a wide range of conditions. In these studies, the wave velocity, current, and attenuation were the most frequently measured quantities. Much of this work is summarized in a review by Vasilyak [40]. Also reviewed are Slavin and Sopin's work which was the first to attempt a computation of the electron energy distribution function EEDF in FIWs [56].

The experimental measurements and computational work reported by Vasilyak were expanded on by a series of studies conducted at the Moscow Institute of Physics. These are

reviewed by Starikovskaia et al. [44] and included measurements of the electron density, electric field, and energy coupling for FIWs in air, nitrogen, and hydrogen. The computational work by Starikoskaia and Starikovskii [57] still represents the most detailed study of the EEDF in nitrogen FIWs.

However, Starikovskaia et al. noted that the usefulness of FIWs were limited, in part, by their repetition rates. The power supplies for FIWs were capacitor banks, charged in parallel, and discharged in series (also referred to Marx banks). Unfortunately, the spark gaps used to trigger these capacitor banks would not operate above a few hundred Hz. This changed in the late 1990's with the development and commercialization of fast, solid-state switches. Specifically, with the fast ionization dynistor it was possible to achieve repetition rates of 100 kHz.

This led to a new class of repetitively-pulsed discharges, or the RPND. These discharges operated at sufficiently high rates such that charged particles would persist between pulses, significantly increasing the plasma duty cycle. The improved qualities of the RPND over the FIW inspired a number of novel, application-driven studies. This included:

- Plasma-assisted combustion [47, 58, 59]
- Magnetohydrodynamic energy bypass engines [48, 59, 60]
- Plasma actuators [49, 61]
- High-pressure xenon lamps [50]
- Plasma medicine [62, 63]
- Water treatment [64]

Though not specific to the RPND, Becker et al. [65] provide an extensive discussion of the potential uses for non-equilibrium air plasmas.

As a result, contemporary researchers have produced a wealth of literature on the operation of RPNDs. More recently, there have been detailed measurements of the gas tempera-

tures [52, 58, 66–71], chemical composition [68–70], electric fields [53, 72, 73], and energy coupling [58, 74]. Notably, these studies have been generally restricted to molecular gases; air, nitrogen, and occasionally, hydrogen.

The first such study was the work of Laroussi and Lu who examined a RPND excited in a stream of helium flowing from a tube into air [75, 76]. The resulting plasma had the appearance of a jet, emitted from the open end of the tube. Using fast photography they observed that the jet was actually a series of plasma "bullets" formed with each pulse. Measurements of the bullet velocities showed that their speed greatly exceed what would be expected purely from electrons drifting under the applied electric field. They described the bullet as a classic cathode-directed streamer propagated by photoionization.

The plasma bullets of Laroussi and Lu spawned a great deal of interest in RPND helium plasma jets[3] For example, Walsh et al. studied the atomic oxygen production for helium-oxygen mixtures with the use of emission spectroscopy and a global plasma chemistry model [79]. Urabe et al. employed a variety of laser diagnostics to measure the radial density profiles of helium metastable atoms and molecular nitrogen ions in a similar jet. This work was supported by a number of two-dimensional plasma simulations such as those by Naidis [80] and Breden, Miki, and Raja [81].

Simultaneously, there has been a decline in the study of FIWS, and relatively little on large-volume RPNDS. One of the most recent FIW studies was produced by Takashima et al. [82]. In it, the authors reported on FIWS in helium and nitrogen which were studied using capacitive probes and voltage-current characteristics. The results were compared to extensive two-dimensional fluid simulations and an analytic, one-dimensional drift model. In most cases, the measurements and simulations showed good agreement.

[3] A distinction should be made between plasma jets, excited by sinusoidal power supplies, similar to the well-known dielectric-barrier discharge [77], and those produced by nanosecond pulses. Differences between the two were reported by Walsh, Shi, and Kong [78].

CHAPTER 2

Theory

2.1 Ionized Gas

A plasma is considered to be a form or subset of ionized gas. That is, a volume of gas in which some fraction of the neutral atoms and/or molecules have been separated into electron and ion pairs. For a sufficiently large number of particles, the behavior of each species in the ionized gas can be described by a continuous distribution function.

This probability distribution expresses the likelihood of finding a particle with a specific range of velocities in a specific volume, as a function of time. This function is denoted as $f_\alpha(\vec{r}, \vec{v}, t)$, where the subscript α denotes the species, f is the probability distribution, $\vec{r}$ is the position, $\vec{v}$ is the velocity, and t is the time.

The behavior of f_α can be shown to be governed by the Boltzmann equation,

$$\frac{\partial f_\alpha}{\partial t} + \vec{v} \cdot \nabla f_\alpha + q_\alpha \left(\vec{E} + \vec{v} \times \vec{B} \right) \cdot \nabla_v f_\alpha = \left(\frac{\partial f_\alpha}{\partial t} \right)_{\text{coll}}. \tag{2.1}$$

Here, q is the charge of the species, $\vec{E}$ is the electric field, $\vec{B}$ is the magnetic field, and $\partial f_\alpha / (\partial t)_{\text{coll}}$ is a term which represents changes to the distribution function as a result of collisions. Coupled with Maxwell's equations, equation 2.1 provides a complete description of the behavior of the fields and particles in a plasma.

For a species in equilibrium in the absence of external forces and $(\partial f_\alpha / \partial t)_{\text{coll}} = 0$, it

can be shown that the distribution of energies is

$$f_\alpha(\varepsilon) = \frac{3\sqrt{3}}{\sqrt{2\pi}}(k_\mathrm{B}T_\alpha)^{-3/2}\exp\left(-\frac{3\varepsilon}{2k_\mathrm{B}T_\alpha}\right) \tag{2.2}$$

where ε is the energy, k_B is Boltzmann's constant, and T_α is the temperature of the species. This is referred to as the Maxwell-Boltzmann distribution. It should be emphasized that this solution only applies when the species can be considered to be in equilibrium. Gradients and electromagnetic fields can both significantly alter the distribution function of a species. This can be of particular importance in the calculation or reaction rates, or the measurement of temperatures.

Additionally, the Boltzmann equation may be solved for electrons, assuming they only interact through elastic collisions, and that they are in equilibrium with a small, constant electric field. This result was originally presented by Druyvesteyn and Penning [83] and has come to be known as the Druyvesteyn distribution. It is defined as,

$$f_\alpha = \frac{3\sqrt{3}}{4\Gamma(3/4)}(k_\mathrm{B}T_\alpha)^{-3/2}\exp\left[-\frac{9}{16}\left(\frac{\varepsilon}{k_\mathrm{B}T_\alpha}\right)\right] \tag{2.3}$$

where Γ is the gamma function. This solution tends to suppress the probability of higher and lower-energy electrons in favor of more intermediate values. Figure 2.1 compares the probably distributions from equations 2.2 and 2.3 for the same temperature α. The dotted line illustrates the average energy for the two distributions, which is not the same as the most probably energy.

Additional solutions of equation 2.1 in anything but these simple cases can be very challenging. In most situations, it is reduced to more tenable equations by integrating over velocity-space (leaving f as a function of space and time). The first so-called moment is often called the conservation equation or continuity equation,

$$\frac{\partial n_\alpha}{\partial t} + \nabla\cdot(n_\alpha\vec{u_\alpha}) = G_\alpha - L_\alpha. \tag{2.4}$$

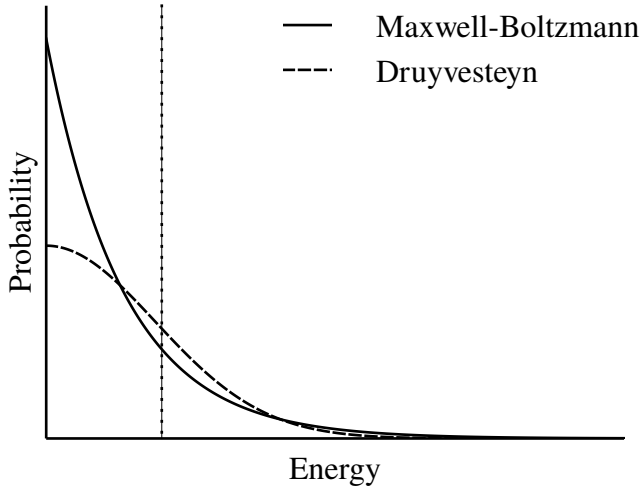

Figure 2.1: Comparison of the Maxwell-Boltzmann energy distribution and the Druyvesteyn distribution for the same average energy (illustrated by the dotted line).

In this case, $\vec{v}$ has been replaced by a mean velocity $\vec{u}$, and the collision operator has been replace by gain (G) and loss (L) terms. The gain and loss terms are generally calculated by integrating a cross section over a known velocity distribution.

The definition of the mean velocity, $\vec{u}$ can be obtained by multiplying equation 2.1 by v and integrating over velocity-space, to obtain the second moment,

$$m_\alpha n_\alpha \left[\frac{\partial \vec{u_\alpha}}{\partial t} + (\vec{u_\alpha} \cdot \nabla)\vec{u_\alpha} \right] = q_\alpha n_\alpha (\vec{E} + \vec{u_\alpha} \times \vec{B}) - \nabla \cdot \vec{\Pi} + \vec{f}|_{\text{coll}}. \tag{2.5}$$

This expresses the conservation of momentum by the plasma. It provides a means by which to solve for the mean velocity of the system, however it also introduces two additional terms. $\vec{f}|_{\text{coll}}$ deals with the forces transferred to α via collisions. Though complex, it only depends on known quantities. The second term, $\vec{\Pi}$, is the pressure tensor and can only be defined by the third moment of the Boltzmann equation. In fact, each additional moment introduces a new term requiring a higher order moment, *ad infinitum*. In most situations, this chain of equations is terminated after the first two or three moments by the use of an additional assumption such as an equation of state.

For our purposes, one more moment will suffice. Assuming that the pressure is isotropic, one can multiply equation 2.1 by $mv^2/2$, and integrate over velocity-space. This yields the energy conservation equation,

$$\frac{\partial}{\partial t}\left(\frac{3}{2}p_\alpha\right) + \nabla\cdot\frac{3}{2}(p_\alpha\vec{u}_\alpha) + p_\alpha\nabla\cdot\vec{u}_\alpha + \nabla\cdot\vec{q}_\alpha = \frac{\partial}{\partial t}\left(\frac{3}{2}p_\alpha\right)\Big|_{\text{coll}}. \tag{2.6}$$

In this case, p represents the isotropic pressure, and $\vec{q}$ is the heat flow. The first term on the LHS represents the total energy contained by the species, the second term is the energy flux in and out of the volume, and the third term accounts for changes due to compression or expansion. The RHS is the collision operator which describes energy added or removed from the system as a result of collisions.

Equations 2.4 and 2.6 are particularly important for this study. As will be detailed in chapter 6, the two can be used to create a global model of the plasma. While such a model only considers globally averaged quantities, it can be extremely useful in characterizing the complex evolution of multi-component plasmas.

2.2 Plasma Criteria

Though the Boltzmann equation can describe both an ionized gas and a plasma, the two are conceptually distinct. A plasma is unique in that its dynamics are governed by long range electromagnetic forces unlike gases in which short-range collisions dominate. As a result, plasmas frequently feature large scale structure and organization. Examples of these structures are ubiquitous in astronomy where phenomena such as the aurora borealis, coronal mass ejections, and even interstellar media all qualify as forms of plasma. How then, does one define a plasma? There are three criteria required for an ionized gas to be considered a plasma.

2.2.1 Debye Length

As mentioned, an ionized gas features a number of electron and ion pairs. If an electrical perturbation is introduced into the ionized gas, the charged particles will tend to rearrange themselves to shield it out. A plasma is an ionized gas which is large enough for this shielding effect to occur. The characteristic length scale for this shielding effect to take place is referred to as the Debye length, denoted λ_D. It can be shown to be equal to $\sqrt{\varepsilon_0 T_e/(en_0)}$, where ε_0 is the vacuum permittivity, T_e is the electron temperature, and n_0 is the plasma density. If the characteristic length scale of the ionized gas is L, then $\lambda_D < L$ for it to be considered a plasma.

2.2.2 Debye Sphere

However, the previous condition is necessary, but not sufficient for shielding to occur. It is possible that an ionized gas may have a relatively small Debye length, but also lack enough charged particles for shield to occur. More simply put, it would be impossible for a single electron to shield out even the smallest of perturbations. For that reason, the number of particles in a Debye sphere must be greater than unity in a plasma, or $n_0(4\pi\lambda_D^3/3) >> 1$.

2.2.3 Plasma Oscillations

Finally, a plasma may exhibit Debye shielding, but lack the long-range interactions of a plasma. This can occur when the collision frequency with neutral particles is too high. In this case, the behavior of the ionized gas would be determined more by the random collisions. Therefore, the characteristic response frequency of a plasma, commonly called the plasma frequency, must be greater than the neutral collision frequency, or $\omega_p > \nu$. The plasma frequency can be shown to be $\omega_p = \sqrt{e^2 n_0/(\varepsilon_0 m_e)}$.

There are many natural and man-made ionized gases which can be considered plasmas. Figure 2.2 shows several categories of plasma, plotted as a function of their electron density

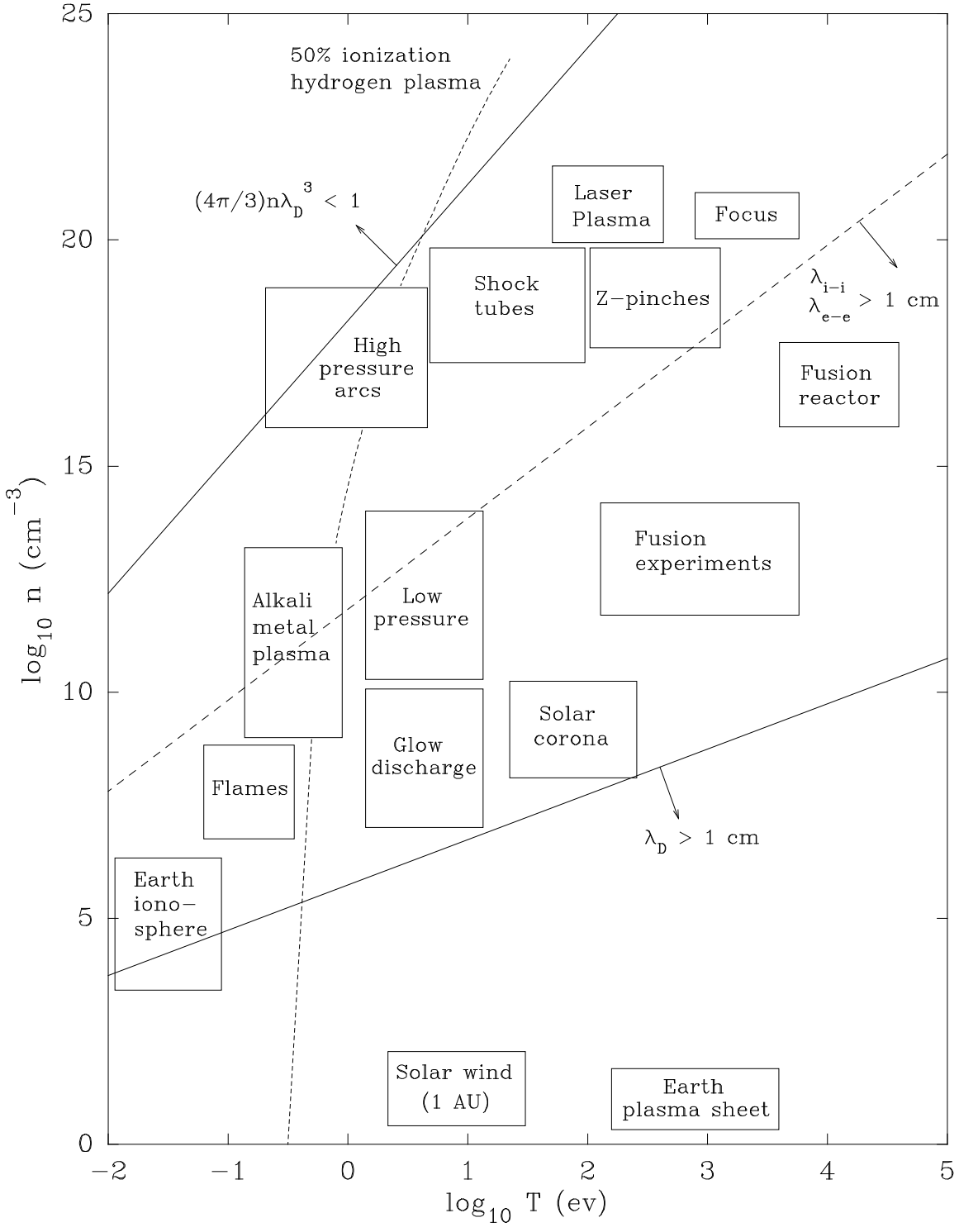

Figure 2.2: Illustration of the various regimes of plasma in terms of electron temperature and density [1].

and temperature. As can be seen, the electron densities span seven decades, and the densities cover in excess of 20. This broad range of conditions presents a particularly challenging problem for both simulations and experimental measurements.

2.3 Discharge Initiation

The Boltzmann equation is a continuous, statistical description of a plasma. By comparison, the initial breakdown of a plasma is a highly discontinuous process marked by its stochasticity. The initiation of a discharge is typically the result of electron avalanches which occur randomly throughout a volume of gas. Often, the seed electrons for a plasma are the products of ionizing cosmic rays which generate a few electrons per cubic-centimeter. As a result, it is necessary to consider the initiation of a discharge separately from a pre-existing plasma.

2.3.1 Townsend Mechanism

Classically, plasmas are created by two different mechanisms, the choice of which depends on the strength of the electric field. At lower electric fields, the Townsend mechanism is responsible for the formation of a plasma. Consider a two electrodes separated by a gap filled with some gas. An electron starting near the cathode will drift toward the anode. For a large enough electric field the electron will gain enough kinetic energy to ionize a neutral atom, producing a second electron. The two electrons are now accelerated by the field, instigating further ionization of the background gas. The population of electrons quickly grows, thus the process is referred to as an electron avalanche. Eventually, the avalanche electrons are collected at the anode.

In their wake are ions which slowly drift toward the cathode. As the ions impact the surface of the cathode, they occasionally cause a secondary electron to be emitted. This secondary electron initiates a new avalanche and helps to sustain the discharge. Townsend

breakdown occurs when the electron multiplication in the avalanche compensates for the finite probability that an ion striking the cathode releases a secondary electron. Therefore, the time required for the ions to drift across the gap is the characteristic time it takes for a discharge to develop via the Townsend mechanism (on the order of 1μs).

The Townsend mechanism is characterized by two parameters: α and γ, the first and second Townsend coefficients. α is the number of ionization events that occur per unit path-length. The value depends on the applied electric field, and is typically expressed in terms of the reduced electric field; the electric field divided by the neutral gas density. The second Townsend coefficient is the probability that an ion impinging on the cathode produces a secondary electron. The values for γ can vary widely and depend on the type of ion, its energy, the cathode material, contamination of the surface, and many other factors. That said, typical values are around 0.01-0.1.

2.3.2 Streamer Mechanism

In contrast, the streamer discharge does not require secondary emission processes. Additionally, streamer discharges can develop in time periods as short as 1 ns, much less than the time required for Townsend breakdown. In order to describe the streamer mechanism, again consider an electron between two electrodes, as seen in (a) of figure 2.3. The electron acquires energy from the applied electric field, and begins to create an avalanche of electrons. The electrons in the avalanche travel with a velocity characterized by the electron mobility, μ. This term expresses the frictional force exerted by the gas on the electrons. Like the first Townsend coefficient, it is a function of the reduced electric field. Consequently, the mean velocity of electrons drifting in a time-varying field $E(t)$ can be expressed as

$$u(t) = \mu(E/N_g)E(t), \tag{2.7}$$

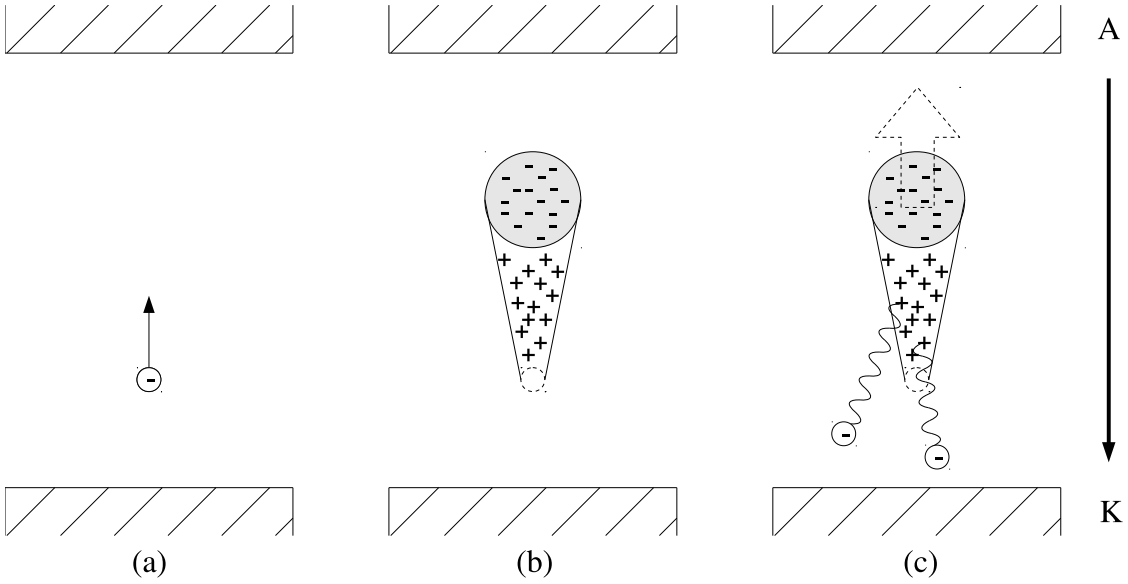

Figure 2.3: An illustration of the development of a single streamer. (a) A seed electron is accelerated by the applied electric field. (b) The initial electron develops into an avalanche which leaves a large region of positive space charge, halting further advance. (c) The streamer propagates toward the cathode via photoionization and the anode via nonlocal electrons and photoionization.

where N_g is the neutral gas density. Given this definition of the electron drift velocity, the total length of the avalanche may be written as

$$\xi = \int_{t_0}^{t} u(t)dt. \tag{2.8}$$

Here, t_0 is the time at which $E(t)$ becomes high enough that the first Townsend coefficient, α, exceeds 0. This is considered the beginning of the avalanche as there is no multiplication before this time.

As seen in figure 2.3, the ions generated by the ionization events remain in place as the electron avalanche passes. This follows from the much larger mass of the ions, and the relatively short time scale on which the avalanche occurs. The cone-like structure of the ions results from the collision-induced, transverse diffusion of the electrons. The free diffusion coefficient is $D = \lambda v_m athrmth(E/N_g)/3$, where λ is the mean free path of the electrons, and $v_{\rm th}$ is their thermal velocity. Following Levatter and Lin [37], if the electrons are assumed

to diffuse equally in all directions, the electron density in the head of the avalanche is

$$n_e(r) = \frac{N_e}{\pi^{3/2} R(t)^2} \exp\left(-\frac{r^2}{R(t)^2}\right), \tag{2.9}$$

where r is the radial coordinate (relative to the center of the avalanche), N_e is the absolute electron population, $\Delta t = t - t_0$, and R is the diffusion radius. The diffusion radius can be calculated from

$$R(t) = \int_0^{\xi} \lambda v_{\mathrm{th}}(\xi') d\xi', \tag{2.10}$$

as the thermal velocity is expected to change as more energy is deposited into the electrons over the length of the avalanche. The dependence of R on time is implied from its dependence on ξ.

In a Townsend discharge, the avalanche would continue across the entire width of the gap. On the other hand, the avalanche of a streamer grows at such a rate that its space charge shields out the applied field. This stalls the head of the avalanche mid-gap as seen in part (c) of figure 2.3. It is commonly assumed that this occurs when the peak field within the head of the avalanche becomes equal to the applied field. Again, from Levatter and Lin, electric field can be found to equal,

$$E_a(r) = \frac{eN_e}{4\pi\varepsilon_0 R^2} F(r/R), \qquad \text{where} \tag{2.11}$$

$$F(r/R) = \frac{1}{R^2}\left[\mathrm{erf}(r/R) - \frac{2}{\pi^{1/2}}(r/R)\exp(-r^2/R^2)\right], \tag{2.12}$$

and erf is the error function. F is a dimenionless function which has a peak value of 0.428. The number of electrons in the avalanche, is equal to

$$N_e = \int_0^{\xi} \alpha(\xi') d\xi'. \tag{2.13}$$

Here, Levatter and Lin make a number of assumptions in order to develop an analytic

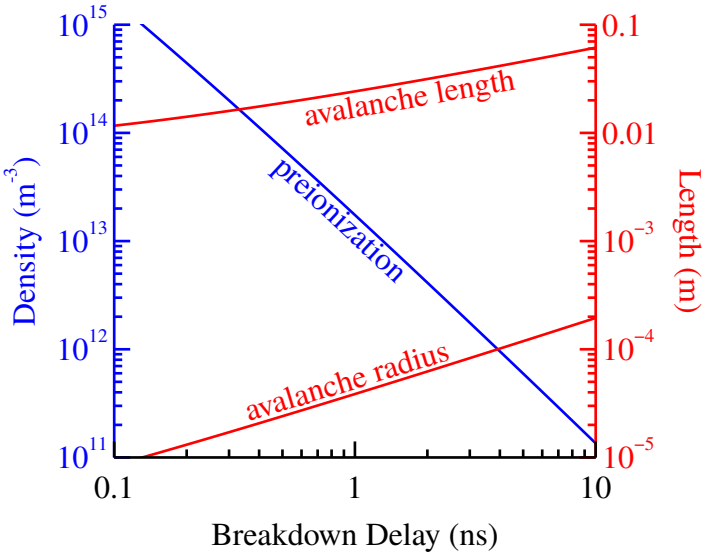

Figure 2.4: Numerical calculations of the preionization density for homogeneous excitation, avalanche length, and avalanche radius in helium at a pressure of 1.0 Torr as a function of the slope of the electric field.

and dimensionless solution for $E_{a,\max}(t) = E(t)$. However, it is possible to numerically integrate equations 2.8 and 2.10 over time until $E_{a,\max}$ is equal to the applied field. This should provide a more accurate, but less general result for the final radius and length of the avalanche. Assuming a linearly increasing electric field, figure 2.4 shows the results of such calculations for an avalanche in 1.0 Torr of helium, as a function of various breakdown delays. The breakdown delay is defined as the time it takes for $\alpha > 0$. The mobilities, mean velocities, and Townsend coefficients were interpolated from solutions of the Boltzmann equation provided by the BOLSIG+ code with Phelps' cross sections [84]. For this range of breakdown delays, the avalanche was able to develop up to 6 cm in length before it stalled. The times required for the avalanche to stall ranged from around 13 ns for the shortest breakdown delay, and 330 ns for the longest.

Once stalled, the avalanche can no longer continue to advance toward either electrode. At this point the avalanche can be considered a streamer as it begins to increase its extent by several other processes. The large internal fields of the avalanche can accelerate individual electrons and "inject" them in the direction of the anode [30]. In addition, as the excited

atoms in the wake of the avalanche begin to radiate, they can cause photoionization throughout the volume. Photoelectrons generated close enough to the negative head, or positive tail of the streamer will initiate secondary avalanches which eventually connect to the primary one. Both of these methods take place primarily along the axis of the original avalanche, thus the streamer remains relatively constricted in the direction transverse to the electric field.

However, these processes are not critical in the formation of a large-volume discharge by an RPND. The previous description of a streamer only considers an avalanche generated by a single electron. In reality, many can form simultaneously assuming that there is more than one seed electron in the volume. With sufficient pre-ionization of the volume, the strong fields of the individual avalanches can begin to overlap. This smoothes out the field gradients which result in constricted streamers and leads to a relatively homogeneous breakdown.

This field overlap is roughly equivalent to a spatial overlap of the heads of the avalanches. In this case, the condition for homogeneous breakdown is simply $n_{e,c} > r_c^{-3}$, where $n_{e,c}$ is the preionization density, and r_c is the radius of the stalled avalanche. A plot of this condition with the breakdown time can also be observed in figure 2.4.

It is apparent that as the avalanche radius increases, the necessary pre-ionization decreases. It is less obvious as to why the avalanche radius decreases as the breakdown delay increases. This can be explained by the lower slope, implied by the long breakdown delays. As the slope decreases, the avalanche has a longer period of time to diffuse in the system, thus the increased radius.

2.4 Atomic Spectroscopy & Notation

Given a particular plasma, it is often desirable to measure various critical parameters. Such measurements can be broadly split into perturbing and non-perturbing measurements. Perturbing measurements, such as those made with physical probes inserted into the plasma,

can alter the local or even global qualities of a plasma. In contrast, non-perturbing measurements, are passive and do not influence the plasma in any way.

A number of non-perturbing diagnostics involve the practice of plasma spectroscopy, or the interaction of light and plasma. Careful measurements of the light emitted from excited atomic states can yield electron densities and temperatures, excited state densities and temperatures, electric fields, and magnetic fields. The topic of spectroscopy is extensive and it is neither necessary nor desirable to cover it in full. Instead we will only consider what is necessary to understand the emissions from a singly-excited, multi-electron atom.

An atom is composed of a small, positively charged nucleus, orbited by negatively charged electrons. The actual position of any single electron is probabilistic and described by a wavefunction; solutions of the Schrödinger equation for the atom in question. Many different wavefunctions or orbitals exist, each described by four quantum numbers:

- $n = 1, 2, \ldots$: the principal quantum number,
- $l = 0, 1, \ldots, n-1$: the orbital angular momentum,
- $m_l = -l, \ldots, l$: the magnetic quantum number, and the
- $s = \pm 1/2$: spin quantum number.

The quantum numbers are hierarchical such that each n, or shell, possesses a series of subshells, l, while each subshell possesses a number of individual states, m_l, and each state possess one of two spins. The Pauli exclusion principle forbids the electrons of an atom from possessing the same combination of quantum numbers. As a result, each subsequent shell of an atom can only contain $2(2l+1)$ electrons, after which it is considered full. The subshells are often referred to using the nomenclature $0, 1, 2, 3, \ldots = s, p, d, f, \ldots$.

As a result of their separation from the nucleus, the electrons in an atom have some degree of potential energy. As the n and l of an electron increase, so does its potential energy. In most cases, m_l and s do not affect the potential energy of an electron. As an

example, an electron in the 1s ($n = 1$ and $l = 0$) subshell has the lowest possible potential energy.

Absent from external influences, the subshells are populated with electrons so as to minimize the total potential energy of the system. This natural arrangement is referred to as the ground state configuration. Often, but not always, the subshells are filled sequentially and in order from lowest to highest l. Provided some input energy, one or more of the electrons surrounding the atom may transition to another orbital, increasing the potential energy of the system. In low-temperature plasmas it usually one of the electrons from the outermost or unfilled subshell to be excited.

In hydrogen and alkali metals, all the subshells are filled with the exception of a lone electron in the outer (or valence) subshell. For these atoms, the potential energy of any singly-excited configuration is uniquely determined by this electron. As a result, the initial and final states of the atom can be uniquely identified based on the initial and final n and l of the aforementioned electron. In contrast, the potential energies of configurations in other atoms are determined by the collective effects of all outer electrons.

This necessitates an additional means of classifying the electron configurations in these atoms. It turns out that the states of these types of atoms can be specified based on their total orbital angular momentum $L = \sum l_i$, the total spin, $S = \sum s_i$, and the total angular momentum, $J = L + S$, where i are all the electrons of the valence shell. In addition, each state can be said to have either even or odd parity, defined as $(-1)^{\sum l_i}$, where -1 is odd, and 1 is even.

Together, these values are sufficient to identify the electron configuration in these atoms. They are often written out in a form called the term symbol which lists the filled subshells and appends a symbol representing the outer subshell configuration. For example, the so called triplet metastable state of helium can be written as $1s2p^3P^o_{0,1,2}$. This describes a helium atom with one electron in the 1s subshell and a second atom in the 2p subshell. This configuration has a total orbital angular moment of 1 (denoted by the 'P'), odd parity

(denoted by the superscript 'o'), a total spin of $1/2$ (the superscript 3 is equal to $2S+1$) and three possible values for the total angular momentum: 0, 1, or 2 which varies depending on the spin-orbit interaction.

These excited atomic states usually have finite lifetimes as the electrons in the excited states will often transition to lower states. This can occur spontaneously, through the emission of a photon, or via a superelastic collision with another particle. In the case of spontaneous transitions, only certain ones are allowed, as defined by a set of selection rules:

- $\Delta S = 0$
- $\Delta L = \pm 1$ or 0
- $\Delta J = \pm 1$ or 0
- $L = 0$ cannot transition to $L = 0$
- $j = 0$ cannot transition to $J = 0$

These rules are determined using the electric dipole approximation. As a result, some transitions forbidden by these rules can occur, though they occur at a much lower rate.

Figure 2.5 is a diagram of the energy levels in neutral helium and the allowed transitions. In this case, the atomic states are separated into the singlet ($S = 0$) and triplet ($S = 1$) manifolds. The singlet manifold represents excited states where the electron spins are anti-parallel, and the triplet manifold represents excited states where the electron spins are parallel. As indicated by the first selection rule, transitions between these two manifolds is forbidden, thus each is something of a self-contained system.

2.4.1 Spectral Lineshapes

It is the transitions between these various excited states which concern spectroscopy. Electrons which transition to lower energy states emit photons which can be detected. Conversely, if an atom is exposed to a photon with an energy matching a transition, the atom

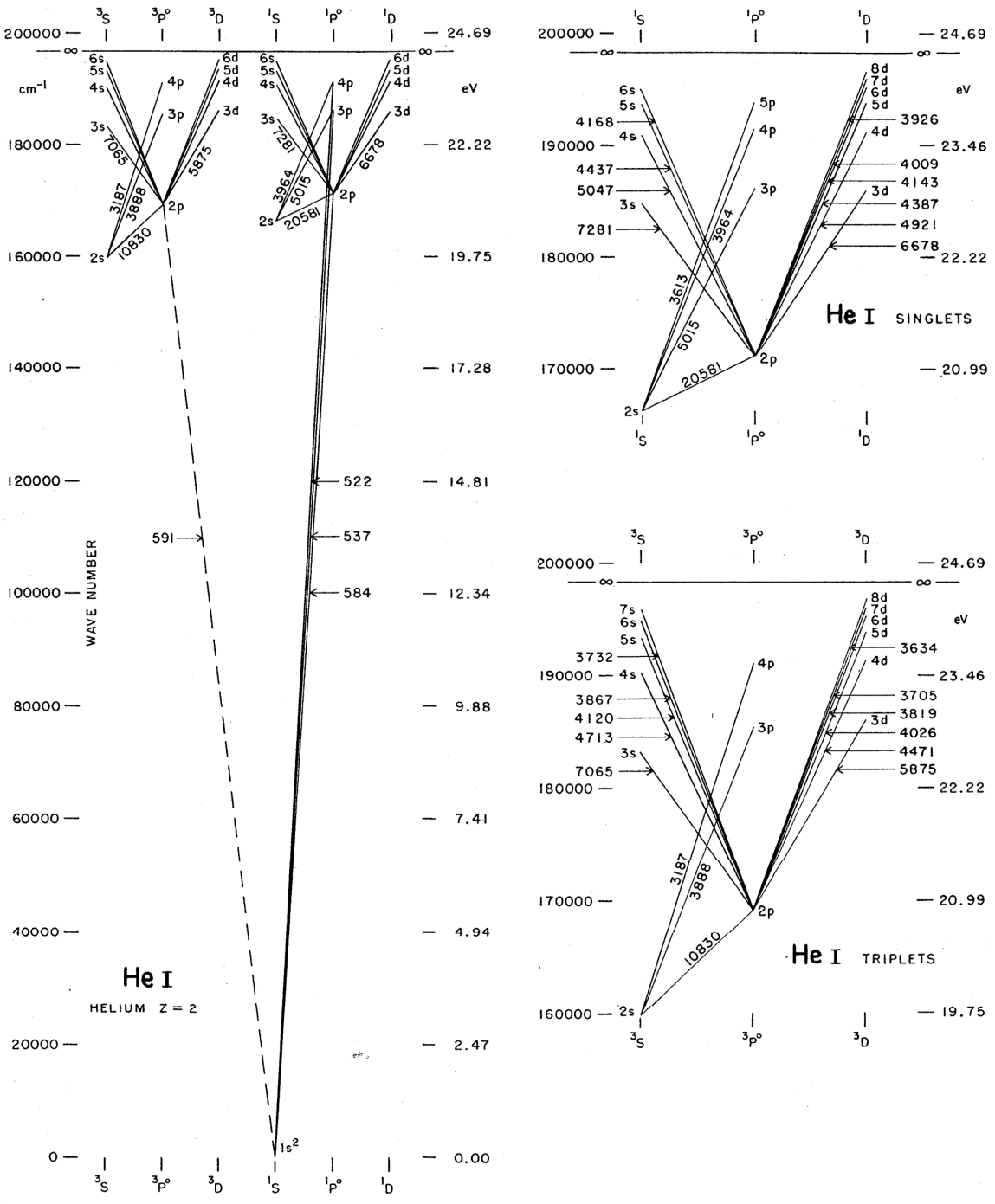

Figure 2.5: A partial Grotrian diagram of neutral helium [2].

may absorb the photon. Both processes are useful in determining the prevalence and dynamics of the excited states. This, in turn, can be used to infer various plasma properties.

Conservation of energy requires that the energy of the absorbed or emitted photon match the energy difference between the two states. However, the finite lifetime of excited atomic states implies, via the time-energy formulation of the uncertainty principle, some uncertainty in the actual energy difference between the states. As a result, the emitted photon will possess an energy selected from a distribution of energies.

This distribution is referred to as the spectral lineshape. The natural lineshape of an atomic transition can be shown [85] to be a Lorentzian of the form,

$$g(\omega) = -\frac{1}{4\pi^2}\frac{A\lambda^3}{\Delta\omega_a}\frac{1}{1+\left[2(\omega-\omega_a)/\Delta\omega_a\right]^2}, \tag{2.14}$$

where ω is the photon frequency, A is the Einstein coefficient for the transition, λ is the wavelength of the transition, ω_a is central frequency of the transition, and $\Delta\omega_a$ the full-width half maximum (FWHM) of the transition. In the ideal case, where the atoms motionless and unaffected by external perturbations, $\Delta\omega_a = A$. This is known as the natural linewidth.

Other processes can affect the spectral lineshape. For example, inter-atomic collisions can reduce the lifetimes of excited states. This results in additional broadening of the line, though it retains its Loretnzian nature. As the frequency of inter-atomic collisions increases linearly with pressure, this phenomena is referred to as pressure broadening. It can be included in equation 2.14 by using $\Delta\omega_a = A + BP$, where B is a measured or calculated broadening coefficient, and P is the pressure.

Atomic motion can also play a role in the spectral lineshape. If an atom is moving toward or away an observer as it emits a photon, the emitted photon will be blue or red shifted. If this effect is averaged over the random motion of atoms in a gas, the result is an additional broadening of the lineshape, called Doppler broadening. Unlike pressure broadening,

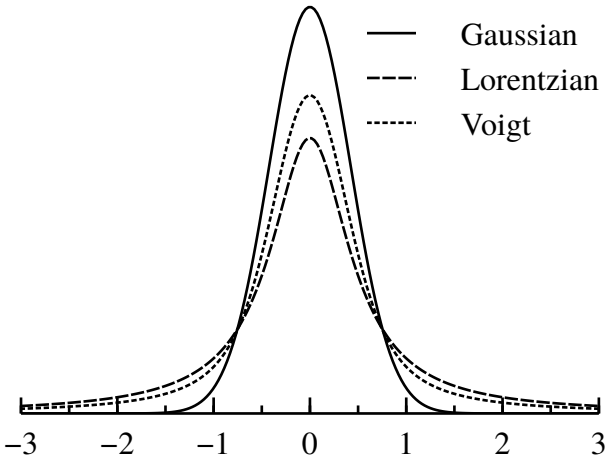

Figure 2.6: A comparison of the three primary spectral lineshapes, each with the same full width.

Doppler broadening introduces a Gaussian component to the lineshape such that,

$$g(\omega) = \sqrt{\frac{2\ln 2}{\pi^3}}\frac{\Delta\omega_a}{\Delta\omega_d}\int_{-\infty}^{\infty}\frac{1}{[(\omega-\omega_a)-\omega']^2+4\Delta\omega_a^2} \times \exp\left[4\ln 2\left(\frac{\omega'}{\Delta\omega_d}\right)^2\right]d\omega'. \quad (2.15)$$

Here, $\Delta\omega_d = \omega_a\sqrt{\frac{8k_B T_g \ln 2}{Mc^2}}$, is the width of the Doppler broadening. This form of the spectral lineshape is known as the Voigt profile, and it must be numerically integrated. In the case that $\Delta\omega_d >> \Delta\omega_a$, equation 2.15 can be simplified to a standard Gaussian distribution,

$$g(\omega) = \sqrt{\frac{4\log 2}{\pi\Delta\omega_d^2}}\exp\left[-(4\log 2)\left(\frac{\omega-\omega_a}{\Delta\omega_d}\right)^2\right]. \quad (2.16)$$

The effect of the various broadening mechanisms is most apparent in the wings of the lineshape, far from the peak. Figure 2.6 illustrates the three major lineshapes with equivalent full widths. The Voigt profile is composed of equally broad Lorentzian and Gaussian distributions. As can be seen, the wings of the Gaussian distribution fall off very quickly.

In comparison, the Lorentzian component is observable well out to the edges of the figure.

The spectral lineshape can be altered by a number of other processes. Electric fields can influence the emissions via the Stark effect, while magnetic fields can split up degenerate states via the Zeeman effect. The fields of electrons and nearby molecules can also alter the lineshape of a transition. While not used in this study, such effects can be used as effective diagnostic tools for plasmas.

CHAPTER 3

Experiment

3.1 Discharge Apparatus

The discharge apparatus geometry was consistent with the design of a coaxial transmission line. This is similar to the design guidelines provided by Vasilyak [40]. The inner conductor is the plasma generated by the fast ionization wave. Surrounding that is a coaxial dielectric, in this case a quartz tube with 2.75" Conflat flanges on either side. Finally, surrounding the dielectric is the outer conductor or shield. In this case, the shield was an aluminum cylinder with slits of approximately 1.5" by 12" milled lengthwise. Figure **??** is a photograph of this discharge apparatus.

One flange of the quartz tube was held at ground potential, while the other flange was pulsed to approximately 7 kV. Given that the plasma undergoes significant decay between pulses, it is assumed that the impedance is almost infinite when the pulse is first applied, thus the actual voltage on the powered electrode is likely closer to 14 kV. The aluminum shield provides the ground connection for the ground electrode. The two were connected using a copper shim and a compressive shaft collar. The aluminum tube was connected to a second ground shield with a one inch copper braid. This second shield was made of copper and was separated by a teflon cylinder, with walls approximately 1" in thickness, from the powered electrode. Figure **??** is a schematic of the discharge apparatus.

Connected to the powered electrode was a Conflat nipple and an angled quartz window

used in the LCIF experiments. A short, silicone-coated, high voltage wire connected the window flange to the central conductor of an HN connector. The HN connector was seated on a square copper plate, which was pressed against the shield using four 10-32 screws.

The HN connector was used to attach the transmission line from the high voltage pulser. Initial experiments attempted to use N connectors, however these were susceptible to breakdown in the air gap which separated the center conductor from the outer shield. The transmission line was approximately 15 m in length. Observations, consistent with calculations, indicated that this provided a window of approximately 140 ns in which to make measurements before the reflected pulse returned to the system and re-energized the plasma.

Attached grounded flange was a second quartz envelope that isolated the ground electrode from the pumping section of the apparatus. Connected to the second quartz envelope was a stainless steel tee, one side of which was connected to an angled quartz window used for the LCIF experiments. The other side of the tee was isolated with an alumina break from a series of Conflat fittings connected to a roughing pump. The roughing pump was connected with a shutoff valve, as well as two bypass lines with inline needle valves for flow regulation.

3.2 Measurement Conditions

LAS, emission, and coupling energy measurements were made at three different operating pressures. The operating pressures were: 0.3, 0.5, 1.0, 2.0, 3.0, 4.0, 8.0, and 16.0 Torr. Pressures below 10.0 Torr were measured with a capacitance manometer with a full scale range of 10.0 Torr, above this a capacitance manometer with a full scale range of 100.0 Torr was used.

Optical measurements were made at three locations along the axis of the discharge. The measurement location closest to the anode was separated from it by a distance of approximately six inches. Each other optical measurement location was moved further from the

anode by an additional three inches.

For each operating condition, measurements were made of the voltage and current. The voltage measurement was made via an internal divider from the power supply. Current measurements were made using an back-current shunt located at a break in the outer shield of the transmission line. The back-current shunt can be seen in Figure **??**. It is composed of nine, low impedance, one ohm resistors, connected in parallel. Each side of the resistors were soldered to a piece of copper foil which was then soldered to the outer shield. A calibrated DC power supply was used to measure the resistance of the current shunt.

All measurements were made using a LeCroy Waverider oscilloscope with a bandwidth of 1 GHz. Connections were made using minimal lengths of RG 50/U cable. When necessary for timing purposes, the cable lengths were matched. Connections were made using minimal lengths of RG 50/U cable. When necessary for timing purposes, the cable lengths were matched. All measurements which required maximum bandwidth were made with a using external 50 ohm terminators.

3.3 Energy Coupling

For comparison to other discharges, estimates of the energy coupling were made using the current and voltage characteristics at each operating pressure.

3.4 Absorption Setup

The LAS setup was based upon the used of a distributed-feedback laser diode. Temperature and current control of the diode provided coarse and fine tuning, respectively, for the output frequency. It was found that it was unnecessary to adjust the temperature for the diode once the correct transition was found, therefore all tuning was accomplished using current tuning.

The laser diode was produced by Toptica Photonics (model #LD-1083-0070-DFB-1), and had a nominal operating power of 70 mW at a center wavelength of 1083 nm. The diode

was held inside a Toptica DL-100 diode housing which contained an integral thermoelectric cooler and collimating optics. The operation of the diode was controlled by a Toptica DC 110 monitor, DCC 110 current control, DTC 110 temperature control, and SC 110 scan control.

A schematic of the optical layout for the absorption experiment can be seen in Figure **??**. Immediately after exiting the housing, the beam was passed through an optical isolator in order to prevent instabilities from back reflections. Next the beam was attenuated using a neutral density filter in order to keep its intensity below the saturation level for the transition. Following that, the beam passed through two apertures for alignment. Here, the beam was split by a partially reflecting mirror. Approximately 98% of the beam was allowed to pass through to a reference photodiode (Thorlabs DET300). After passing through the plasma, entered another aperture to limit near-coincident plasma emissions. The background emissions were further reduced using a long pass filter with a cutoff of 1000 nm. Finally, the beam was coupled into an optical fiber which connected to the detection electronics.

The transmitted laser light was detected with an InGaAs photodiode (Thorlabs DET410). The signal from the diode was often too small to detect, so the output of the signal photodiode was sent through a voltage amplifier (Femto HVA-200M-40-B). The light response of this system is limited by the photodiode which has a nominal rise time of five nanoseconds. The signal from the amplifier was terminated by a 50 ohm terminator and sensed by the aforementioned oscilloscope.

3.4.1 Acquisition Process

The actual acquisition process required a specific series of steps in order to properly account for all noise sources. In order to accommodate this process, a custom LabView script was used to automate the acquisition of the laser transmission spectra. Generally speaking, the

signal can be described as

$$V_{\text{total}} = V_{\text{signal}} + V_{\text{background}} + V_{\text{plasma}}. \tag{3.1}$$

In order to remove the background signal, the acquisition scr

3.5 Emissions Setup

CHAPTER 4

Metastable Measurements

CHAPTER 5

Emission Measurements

CHAPTER 6

Modeling

CHAPTER 7

Conclusions

APPENDIX A

Millimeter-Wave Interferometry

APPENDIX B

Rotational Spectroscopy

Previous studies have found that ionization waves can induce fast gas heating in molecular gas systems [86]. Up to 40% of the input energy can be converted into translational energy through dissociation of oxygen and quenching or electronically excited nitrogen states. In combustion applications, this gas heating can play an important role in the combustion chemistry, flame holding, and ignition delay. Likewise, gas heating can impact material processing and ionization efficiency in other RPND applications. As such, it is important to develop reliable temperature diagnostics for RPNDs in molecular gases.

As early as 2001, researchers have proposed the use of a novel, hybrid engine design for use in supersonic and hypersonic flight [87]. Like an earlier program which advertised the use of a magnetohydrodynamic (MHD) accelerator for controlling the gas inlet of a scramjet [88]. Essentially, a hypersonic flow would be ionized by some external source, and used as the working fluid in a downstream MHD generator. The electrical power produced by this system could be used for onboard electronics and subsequent acceleration stages. The slowed flow could then be used with a traditional turbojet engine.

One of the primary difficulties in the development of this MHD energy bypass engine was the efficient ionization of the inlet flow. Originally, Macheret suggested the use of electron beams, carefully tuned to coincide with the peak in the ionization cross section. However, the use of electron beams in the ionization of high pressure gases is accompanied by a large number of technical issues, similar to those some excimer lasers. Therefore, in 2006,

Nishihara et al. proposed the use of an RPND to produce an "electron beam" in situ [67].

B.1 Experiment

B.2 Theory

Researchers at have proposed the use of a novel hybrid engine for supersonic and hypersonic flight [].

The measurement of rotational spectra has been used several

BIBLIOGRAPHY

[1] J D Huba. *NRL Plasma Formulary*. Naval Research Laboratory, Washington, D.C., 2011.

[2] Charlotte E Moore and Paul W Merrill. Partial Grotrian Diagrams of Astrophysical Interest. Technical report, National Bureau of Standards, Washington, D.C., 1968.

[3] Plasma 2010 Committee, Plasma Science Committee, and National Research Councial. *Plasma Science: Advancing Knowledge in the National Interest*. Number 2007. The National Academies Press, Washington, D.C., 2007.

[4] L B Loeb. Ionizing Waves of Potential Gradient: Luminous pulses in electrical breakdown, with velocities a third that of light, have a common basis. *Science (New York, N.Y.)*, 148(3676):1417–26, June 1965.

[5] J J Thomson. *Notes on Recent Researches in Electricity and Magnetism*. Clarendon Press, Oxford, UK, 1893.

[6] C. Wheatstone. Versuche, die Geschwindigkeit der Elektricität und die Dauer des elektrischen Lichts zu messen. *Annalen der Physik und Chemie*, 110(3):464–480, 1835.

[7] W. v. Zahn. Spectralröhren mit longitudinaler Durchsicht. *Annalen der Physik und Chemie*, 244(12):675–675, 1879.

[8] John James. Die Abraham-Lemoinesche Methode zur Messung sehr kleiner Zeitintervalle und ihre Anwendung zur Bestimmung der Richtung und Geschwindigkeit der Entladung in Entladungsröhren. *Annalen der Physik*, 320(15):954–987, 1904.

[9] R. Whiddington. The Discharge of Electricity through Vacuum Tubes. *Nature*, 116(2918):506–509, October 1925.

[10] J. Beams. The Time Interval Between the Appearance of Spectrum Lines in Spark and in Condensed Discharges. *Physical Review*, 28(3):475–480, September 1926.

[11] B. F. J. Schonland and H. Collens. Development of the Lightning Discharge. *Nature*, 132(3332):407–408, September 1933.

[12] a. M. Cravath and L. B. Loeb. The Mechanism of the High Velocity of Propagation of Lightning Discharges. *Physics*, 6(4):125, 1935.

[13] L. Snoddy, J. Beams, and J. Dietrich. The Propagation of Potential in Discharge Tubes. *Physical Review*, 50(5):469–471, September 1936.

[14] E. Flegler and H. Raether. Der elektrische Durchschlag in Gasen nach Untersuchungen mit der Nebelkammer. *Zeitschrift f r Physik*, 99(9-10):635–642, September 1936.

[15] Leonard B. Loeb and John M. Meek. The Mechanism of Spark Discharge in Air at Atmospheric Pressure. I. *Journal of Applied Physics*, 11(6):438, June 1940.

[16] Leonard B. Loeb and J. M. Meek. The Mechanism of Spark Discharge in Air at Atmospheric Pressure. II. *Journal of Applied Physics*, 11(7):459, 1940.

[17] J. Meek. A Theory of Spark Discharge. *Physical Review*, 57(8):722–728, April 1940.

[18] L. Fisher and B. Bedderson. Formative Time Lags of Spark Breakdown in Air in Uniform Fields at Low Overvoltages. *Physical Review*, 81(1):109–114, January 1951.

[19] G. Kachickas and L. Fisher. Formative Time Lags of Uniform Field Breakdown in N2. *Physical Review*, 88(4):878–883, November 1952.

[20] G. Kachickas and L. Fisher. Formative Time Lags of Uniform Field Breakdown in Argon. *Physical Review*, 91(4):775–779, August 1953.

[21] EE Kunhardt and Y Tzeng. Development of an electron avalanche and its transition into streamers. *Physical review. A*, 38(3):1410–1421, August 1988.

[22] I D Chalmers. The transient glow discharge in nitrogen and dry air. *Journal of Physics D: Applied Physics*, 4(8):1147–1151, August 1971.

[23] W Rogowski, E. Flegler, and R. Tamm. Über Wanderwelle und Durchschlag. *Archiv für Elektrotechnik*, 18(5):479–512, September 1927.

[24] K. Buss. Der Stufendurchschlag. *Archiv für Elektrotechnik*, 26(4):266–272, April 1932.

[25] T E Allibone and J M Meek. The Development of the Spark Discharge. II. *Proceedings of the Royal Society A: Mathematical, Physical and Engineering Sciences*, 169(937):246–268, December 1938.

[26] T. E. Allibone and J. M. Meek. The Development of the Spark Discharge. *Proceedings of the Royal Society A: Mathematical, Physical and Engineering Sciences*, 166(924):97–126, May 1938.

[27] T E Allibone. The Mechanism of a Long Spark. *Journal of the Institute of Electrical Engineers*, 82(497):513–521, 1938.

[28] T E Allibone. Development of the Spark Discharge. *Nature*, 161(4103):970–971, June 1948.

[29] R F Saxe and J M Meek. Development of Spark Discharges. *Nature*, 162(4111):263–264, August 1948.

[30] E Kunhardt and W Byszewski. Development of overvoltage breakdown at high gas pressure. *Physical Review A*, 21(6):2069–2077, June 1980.

[31] Yu. L. Stankevich and V. G. Kalinin. Fast Electrons and X-Ray Radiation during the Initial Stage of Growth of a Pulsed Spark Discharge in Air. *Soviet Physics Doklady*, 12, 1968.

[32] Gennadii A Mesyats, Yu I Bychkov, and V V Kremnev. Pulsed nanosecond electric discharges in gases. *Soviet Physics Uspekhi*, 15(3):282–297, March 1972.

[33] L P Babich, T. V. Loiko, and L. V. Tarasova. The physics of high-voltage nanosecond discharges in dense gases. *Radiophysics and Quantum Electronics*, 20(4):436–442, April 1977.

[34] Leonid P Babich, T V Loĭko, and V A Tsukerman. High-voltage nanosecond discharge in a dense gas at a high overvoltage with runaway electrons. *Soviet Physics Uspekhi*, 33(7):521–540, July 1990.

[35] C. a. Fenstermacher. Electron-Beam-Controlled Electrical Discharge as a Method of Pumping Large Volumes of CO2 Laser Media at High Pressure. *Applied Physics Letters*, 20(2):56, 1972.

[36] a. Jay Palmer. A physical model on the initiation of atmospheric-pressure glow discharges. *Applied Physics Letters*, 25(3):138, 1974.

[37] Jeffrey I. Levatter and Shao-Chi Lin. Necessary conditions for the homogeneous formation of pulsed avalanche discharges at high gas pressures. *Journal of Applied Physics*, 51(1):210, 1980.

[38] R O Hunter. Electron beam controlled switching. In *International Pulsed Power Conference*, pages IC8–1 –IC8–6, New York, NY, 1976. Institute of Electrical Engineers, Inc.

[39] B M Koval'chuk and G A Mesyats. Rapid cutoff of a high current in an electron-beam-excited discharge. *Soviet Technical Physics Letters*, 2(252), 1976.

[40] L M Vasilyak, S V Kostyuchenko, N N Kudryavtsev, and I V Filyugin. Fast ionisation waves under electrical breakdown conditions. *Physics-Uspekhi*, 37(3):247–268, March 1994.

[41] N B Anikin, S V Pancheshnyi, S M Starikovskaia, and A Yu Starikovskii. Breakdown development at high overvoltage: electric field, electronic level excitation and electron density. *Journal of Physics D: Applied Physics*, 31(7):826–833, April 1998.

[42] S.V. Pancheshnyi, S.M. Starikovskaia, and A.Yu. Starikovskii. Measurements of rate constants of the v =0) and v =0) deactivation by N2, O2, H2, CO and H2O molecules in afterglow of the nanosecond discharge. *Chemical Physics Letters*, 294(6):523–527, September 1998.

[43] S M Starikovskaia, a Yu Starikovskii, and D V Zatsepin. The development of a spatially uniform fast ionization wave in a large discharge volume. *Journal of Physics D: Applied Physics*, 31(9):1118–1125, May 1998.

[44] S M Starikovskaia, N B Anikin, S V Pancheshnyi, D V Zatsepin, and A Yu Starikovskii. Pulsed breakdown at high overvoltage: development, propagation and energy branching. *Plasma Sources Science and Technology*, 10(2):344–355, May 2001.

[45] S V Pancheshnyi, S M Starikovskaia, and A Yu Starikovskii. Population of nitrogen molecule electron states and structure of the fast ionization wave. *Journal of Physics D: Applied Physics*, 32(17):2219–2227, September 1999.

[46] V.M. Efanov, V.V. Karavaev, A.F. Kardo-Sysoev, and I.G. Tchashnikov. Fast ionization dynistor (FID)-a new semiconductor superpower closing switch. In *Digest of Technical Papers. 11th IEEE International Pulsed Power Conference (Cat. No.97CH36127)*, volume 2, pages 988–991. IEEE, 1997.

[47] S M Starikovskaia. Plasma assisted ignition and combustion. *Journal of Physics D: Applied Physics*, 39(16):R265–R299, August 2006.

[48] S.O. Macheret, M.N. Shneider, and R.B. Miles. Modeling of air plasma generation by repetitive high-voltage nanosecond pulses. *IEEE Transactions on Plasma Science*, 30(3):1301–1314, June 2002.

[49] Igor V Adamovich, Munetake Nishihara, Inchul Choi, Mruthunjaya Uddi, and Walter R Lempert. Energy coupling to the plasma in repetitive nanosecond pulse discharges. *Physics of Plasmas*, 16(11):113505, 2009.

[50] Dmitry S. Nikandrov, Lev D. Tsendin, Vladimir I. Kolobov, and Robert R. Arslanbekov. Theory of Pulsed Breakdown of Dense Gases and Optimization of the Voltage Waveform. *IEEE Transactions on Plasma Science*, 36(1):131–139, 2008.

[51] L D Tsendin and D S Nikandrov. An analytical approach to planar ionization fronts in dense gases. *Plasma Sources Science and Technology*, 18(3):035007, August 2009.

[52] Yvette Zuzeek, Inchul Choi, Mruthunjaya Uddi, Igor V Adamovich, and Walter R Lempert. Pure rotational CARS thermometry studies of low-temperature oxidation kinetics in air and ethene–air nanosecond pulse discharge plasmas. *Journal of Physics D: Applied Physics*, 43(12):124001, March 2010.

[53] Osaka University) Ito, Tsuyohito (Frontier Research Base For Global Young Researchers, Osaka University) Kobayashi, Kazunobu (Center For Atomic And Molecular Technologies, Ruhr-University Bochum) Czarnetzki, Uwe (Institute For Plasma

And Atomic Physics, and Osaka University) Hamaguchi, Satoshi (Center For Atomic And Molecular Technologies. Rapid formation of electric field profiles in repetitively pulsed high-voltage high-pressure nanosecond discharges. *Journal of Physics D: Applied Physics*, 43(6):062001, February 2010.

[54] Tsuyohito Ito, Kazunobu Kobayashi, Sarah Müller, Uwe Czarnetzki, and Satoshi Hamaguchi. Electric field measurements at near-atmospheric pressure by coherent Raman scattering of laser beams. *Journal of Physics: Conference Series*, 227:012018, May 2010.

[55] Brandon Weatherford, Edward Barnat, Zhongmin Xiong, and Mark Kushner. Two-Dimensional Electron and Metastable Density Profiles Produced in Helium Fast Ionization Wave Discharges. *Bulletin of the American Physical Society*, Volume 57,, October 2012.

[56] B B Slavin and P I Sopin. Breakdown of a neutral gas by ionizing waves of the gradient of a negative potential. *High Temperature1*, 30(1):1–9, 1992.

[57] S M Starikovskaia and A Yu Starikovskii. Numerical modelling of the electron energy distribution function in the electric field of a nanosecond pulsed discharge. *Journal of Physics D: Applied Physics*, 34(23):3391–3399, December 2001.

[58] Sergey V. Pancheshnyi, Deanna A. Lacoste, Anne Bourdon, and Christophe O. Laux. Ignition of Propane–Air Mixtures by a Repetitively Pulsed Nanosecond Discharge. *IEEE Transactions on Plasma Science*, 34(6):2478–2487, December 2006.

[59] Igor V. Adamovich, Walter R. Lempert, Munetake Nishihara, J. William Rich, and Yurii G. Utkin. Repetitively Pulsed Nonequilibrium Plasmas for Magnetohydrodynamic Flow Control and Plasma-Assisted Combustion. *Journal of Propulsion and Power*, 24(6):1198–1215, November 2008.

[60] Steven J Schneider, Hani Kamhawi, and Isaiah M Blankson. Efficient Ionization Investigation for Flow Control and Energy Extraction. *AIAA 47th Aerospace Sciences Meeting*, 2009.

[61] A Yu Starikovskii, A A Nikipelov, M M Nudnova, and D V Roupassov. SDBD plasma actuator with nanosecond pulse-periodic discharge. *Plasma Sources Science and Technology*, 18(3):034015, August 2009.

[62] H Ayan, D Staack, G Fridman, A Gutsol, Y Mukhin, A Starikovskii, A Fridman, and G Friedman. Application of nanosecond-pulsed dielectric barrier discharge for biomedical treatment of topographically non-uniform surfaces. *Journal of Physics D: Applied Physics*, 42(12):125202, June 2009.

[63] J L Zimmermann, T Shimizu, H-U Schmidt, Y-F Li, G E Morfill, and G Isbary. Test for bacterial resistance build-up against plasma treatment. *New Journal of Physics*, 14(7):073037, July 2012.

[64] John E. Foster, Grigory Adamovsky, Sarah Nowak Gucker, and Isaiah M. Blankson. A Comparative Study of the Time-Resolved Decomposition of Methylene Blue Dye Under the Action of a Nanosecond Repetitively Pulsed DBD Plasma Jet Using Liquid Chromatography and Spectrophotometry. *IEEE Transactions on Plasma Science*, 41(3):503–512, March 2013.

[65] K H Becker, U Kogelschatz, K H Schoenbach, and R J Barker. *Non-Equilibrium Air Plasmas at Atmospheric Pressure*. Institute of Physics Publishing, Bristol, UK, 2005.

[66] Guillaume Pilla, David Galley, Deanna a. Lacoste, Franois Lacas, Denis Veynante, and Christophe O. Laux. Stabilization of a Turbulent Premixed Flame Using a Nanosecond Repetitively Pulsed Plasma. *IEEE Transactions on Plasma Science*, 34(6):2471–2477, December 2006.

[67] Munetake Nishihara, J. William Rich, Walter R Lempert, Igor V Adamovich, and Sivaram Gogineni. Low-temperature M=3 flow deceleration by Lorentz force. *Physics of Fluids*, 18(8):086101, 2006.

[68] Ainan Bao, Yurii G. Utkin, Saurabh Keshav, Guofeng Lou, and Igor V. Adamovich. Ignition of Ethylene–Air and Methane–Air Flows by Low-Temperature Repetitively Pulsed Nanosecond Discharge Plasma. *IEEE Transactions on Plasma Science*, 35(6):1628–1638, December 2007.

[69] Guofeng Lou, Ainan Bao, Munetake Nishihara, Saurabh Keshav, Yurii G Utkin, J William Rich, Walter R Lempert, and Igor V Adamovich. Ignition of premixed hydrocarbon–air flows by repetitively pulsed, nanosecond pulse duration plasma. *Proceedings of the Combustion Institute*, 31(2):3327–3334, January 2007.

[70] David Z Pai, Gabi D Stancu, Deanna a Lacoste, and Christophe O Laux. Nanosecond repetitively pulsed discharges in air at atmospheric pressure—the glow regime. *Plasma Sources Science and Technology*, 18(4):045030, November 2009.

[71] Munetake Nishihara, Keisuke Udagawa Takashima, John R. Bruzzese, Igor V. Adamovich, and Datta Gaitonde. Experimental and Computational Studies of Low-Temperature Mach 4 Flow Control by Lorentz Force. *Journal of Propulsion and Power*, 27(2):467–476, March 2011.

[72] Tsuyohito Ito, Dirk Luggenhölscher, Kazunobu Kobayashi, Sarah Müller, Uwe Czarnetzki, and Satoshi Hamaguchi. Electric field measurement in an atmospheric or higher pressure gas by coherent Raman scattering of nitrogen. *Journal of Physics D: Applied Physics*, 42(9):092003, May 2009.

[73] Sarah Müller, Dirk Luggenhölscher, and Uwe Czarnetzki. Ignition of a nanosecond-pulsed near atmospheric pressure discharge in a narrow gap. *Journal of Physics D: Applied Physics*, 44(16):165202, April 2011.

[74] S. O. Macheret, M. N. Shneider, and R. C. Murray. Ionization in strong electric fields and dynamics of nanosecond-pulse plasmas. *Physics of Plasmas*, 13(2):023502, 2006.

[75] M. Laroussi and X. Lu. Room-temperature atmospheric pressure plasma plume for biomedical applications. *Applied Physics Letters*, 87(11):113902, 2005.

[76] XinPei Lu and Mounir Laroussi. Dynamics of an atmospheric pressure plasma plume generated by submicrosecond voltage pulses. *Journal of Applied Physics*, 100(6):063302, 2006.

[77] Ulrich Kogelschatz. Dielectric-Barrier Discharges: Their History, Discharge Physics, and Industrial Applications. *Plasma Chemistry and Plasma Processing*, 23(1):1–46, 2003.

[78] J. L. Walsh, J. J. Shi, and M. G. Kong. Submicrosecond pulsed atmospheric glow discharges sustained without dielectric barriers at kilohertz frequencies. *Applied Physics Letters*, 89(16):161505, 2006.

[79] J L Walsh, D X Liu, F Iza, M Z Rong, and M G Kong. Contrasting characteristics of sub-microsecond pulsed atmospheric air and atmospheric pressure helium–oxygen glow discharges. *Journal of Physics D: Applied Physics*, 43(3):032001, January 2010.

[80] G V Naidis. Modelling of streamer propagation in atmospheric-pressure helium plasma jets. *Journal of Physics D: Applied Physics*, 43(40):402001, October 2010.

[81] Doug Breden, Kenji Miki, and Laxminarayan L. Raja. Computational study of cold atmospheric nanosecond pulsed helium plasma jet in air. *Applied Physics Letters*, 99(11):111501, 2011.

[82] Keisuke Takashima, Igor V. Adamovich, Zhongmin Xiong, Mark J. Kushner, Svetlana Starikovskaia, Uwe Czarnetzki, and Dirk Luggenhölscher. Experimental and modeling analysis of fast ionization wave discharge propagation in a rectangular geometry. *Physics of Plasmas*, 18(8):083505, 2011.

[83] M. J. Druyvesteyn and F. M. Penning. The Mechanism of Electrical Discharges in Gases of Low Pressure. *Reviews of Modern Physics*, 12(2):87–174, April 1940.

[84] A V Phelps. Compilation of Electron Cross Sections, 2002.

[85] A. E. Siegman. *Lasers*. University Science Books, Sausalito, CA, 1986.

[86] N a Popov. Fast gas heating in a nitrogen–oxygen discharge plasma: I. Kinetic mechanism. *Journal of Physics D: Applied Physics*, 44(28):285201, July 2011.

[87] Sergey O Macheret, Ronald J Lipinski, Richard B Miles, and Mikhail N Shneider. Electron-Beam-Generated Plasmas in Hypersonic Magnetohydrodynamic Channels. *AIAA Journal*, 39(6):1127–1138, June 2001.

[88] Evgeniy P Gurijanov and Phillip T Harsha. AJAX: New Directions in Hypersonic Technology. In *International Space Planes and Hypersonic Systems and Technologies*, pages 1–9, Seal Beach, CA, 1996. AIAA.